Impact of Western Pacific Subtropical High on Ozone Pollution over Eastern China

Zhongjing Jiang[1], Jing Li[1], Xiao Lu[2], Cheng Gong[3], Lin Zhang[1], Hong Liao[4]

1 Department of Atmospheric and Oceanic Sciences, School of Physics, Peking University, Beijing, China

2 School of Engineering and Applied Sciences, Harvard University, Cambridge, USA

3 Institute of Atmospheric Physics, Chinese Academy of Sciences, Beijing, China

4 Jiangsu Key Laboratory of Atmospheric Environment Monitoring and Pollution Control, Jiangsu Collaborative Innovation Center of Atmospheric Environment and Equipment Technology, School of Environmental Science and Engineering, Nanjing University of Information Science and Technology, Nanjing, China

†Corresponding author: jing-li@pku.edu.cn

Abstract

Surface ozone is a major pollutant in Eastern China, especially during the summer season. The formation of surface ozone pollution highly depends on meteorological conditions largely controlled by regional circulation patterns, which can modulate ozone concentrations by influencing the emission of the precursors, the chemical production rates, and regional transport. Here we show that summertime ozone pollution over Eastern China is distinctly modulated by the variability of West Pacific Subtropical High (WPSH), a major synoptic system that controls the summertime weather conditions of East Asia. Composite and regression analyses indicate that positive WPSH anomaly is associated with higher than normal surface ozone concentration over Northern China but lower ozone over Southern China. Stronger than normal WPSH leads to higher temperatures, stronger solar radiation at the land surface, lower relative humidity, and less precipitation in Northern China, favoring the production and accumulation of surface ozone. In contrast, all meteorological variables show reverse changes in Southern China under stronger WPSH. GEOS-Chem simulations reasonably reproduce the observed ozone changes associated with the WPSH and support the statistical analyses. We further conduct a budget diagnosis to quantify the detailed contributions of chemistry, transport, mixing, and convection processes. The result shows that chemistry act as a decisive role in leading the ozone changes among these processes. Results show that the changes in ozone are primarily attributed to chemical processes. Moreover, the natural emission of precursors from biogenic and soil sources, a major component influencing the chemical production, accounts for ~30% of the total surface ozone changes.

Key words:

Surface ozone, WPSH, meteorological fields, GEOS-Chem, precursor

1. Introduction

Surface ozone is a major trace gas in the lower atmosphere. It is produced by photochemical oxidation of carbon monoxide (CO) and volatile organic compounds (VOCs) in the presence of nitrogen oxides ($NOx=NO+NO_2$) and sunlight. Not only does it act as a greenhouse gas but it also exerts detrimental effects on both human health and the ecosystem (Heck et al., 1983; Tai et al., 2014; Monks et al., 2015; Fleming et al., 2018; Mills et al., 2018; Liu et al., 2018; Maji et al., 2019). In China, the problem of tropospheric ozone pollution is severe in most urban areas, such as the North China Plain (NCP), the Yangtze River Deltas (YRD), and Pearl River Deltas (PRD) (Li et al., 2019; Lu et al., 2018; Silver et al., 2018; Yin et al., 2019). Typically, surface ozone concentration reaches its peak in the summer season due to active photochemistry (Wang et al., 2017; Lu et al., 2018). The summertime daily maximum 8 h average (MDA8) ozone concentrations frequently reach or exceed the Grade Ⅱ national air quality standard of 82 ppbv in NCP (Lu et al., 2018; Ministry of Environmental Protection of the People's Republic of China (MEP), 2012). Moreover, recent studies showed that surface ozone concentration had exhibited an increasing trend since 2013 over most parts of China (Li et al., 2019; Lu et al., 2020).

Surface ozone concentration is distinctly influenced by meteorological conditions, which impact the production, transport, and removal of ozone (Lu et al., 2019a). For example, solar radiation changes surface ozone via the effects on photolysis rates as well as on biogenic emissions. High temperature tends to enhance ozone pollution through stagnant air masses, thermal decomposition of peroxyacetylnitrate (PAN), and the increase of biogenic emissions (Fehsenfeld et al., 1992; Guenther et al., 2012; Rasmussen et al., 2012). Wind speed is generally anticorrelated with surface ozone, indicating the important role of horizontal wind in pollutant dispersion (Zhang et al., 2015; Gong and Liao, 2019). Moreover, the variabilities of these meteorological variables are not independent but interconnected. The synchronous variation of some meteorological variables can be ascribed to the same synoptic weather pattern, thus increasing efforts have been devoted to identifying the synoptic weather patterns that enhance ozone pollution (Gong and Liao, 2019; Liu et al., 2019; Han et al., 2020). For example, Liu et al. (2019) objectively identified 26 weather types, including some that led to highly polluted days, and proved that synoptic changes account for 39.2% of the interannual increase in the domain-averaged O_3 from 2013 to 2017. Han et al. (2020) also identified six predominant synoptic weather patterns over eastern China in summer to examine the synoptic influence of weather conditions on ozone.

A dominant system that affects the summertime weather pattern in China is the WPSH. As an essential component of the East Asia summer monsoon, its intensity, shape, and location control the large-scale quasi-stationary frontal zones in East Asia (Huang et al., 2018). WPSH can significantly influence the monsoon circulation, typhoon tracks, and moisture transport (Choi et al., 2019; Gao et al., 2014) and further impact surface ozone in China. Shu et al. (2016) showed stronger WPSH would increase ozone pollution over YRD by enhancing the ozone production as well as trapping the ozone in the boundary layer. Using observations from 2014 to 2016, Zhao and Wang (2017) indicated that stronger WPSH in summer leads to a decrease in surface ozone in Southern China but an increase in Northern China through statistical analysis. While these studies arrived at qualitative conclusions, they either focused on a limited region or a short time span, and both lacked a comprehensive investigation of the mechanisms through model simulation. Considering the increasingly severe ozone pollution in China, it is desirable to further investigate this topic systematically.

For this purpose, this study aims to address how and why summertime surface ozone concentration in Eastern China responds to changes in the WPSH. A joint statistical analysis and model simulation using the GEOS-Chem is performed to reveal their relationship as well as to examine changes in the relevant chemical and physical processes, in order to provide insights into the formation of summertime ozone pollution in China and to shed light on ozone simulation and prediction.

2. Data and methods

2.1. Surface ozone and meteorological data

Routine daily monitoring of air quality in China became available in 2013, with the establishment of a national network by the China National Environmental Monitoring Centre. The ozone data follows the standard released by the Chinese standard document HJ 654-2013 (MEP, 2013) and the pollutant concentration data is available at https://quotsoft.net/air/. We downloaded hourly surface ozone concentration data for all sites from 2014 to 2018. An ad hoc quality control protocol was developed to remove outliers and invalid measurements (see supplementary information and Figure S1 for examples of outliers). MDA8 was calculated based on the hourly ozone data. We removed the linear trend of the data and converted the data unit from μg m^{-3} into ppbv for further analysis.

Meteorological fields for 2014-2018 were obtained from the Goddard Earth Observing System Forward Processing (GEOS-FP) database (GEOS-FP file specification document, Version 1.0 (11 Jun 2013)), which is the current operational met data product from the Global Modeling and Assimilation Office (GMAO). The data is available at http://ftp.as.harvard.edu/gcgrid/data/GEOS_2x2.5/GEOS_FP. The meteorological variables used include sea level pressure (SLP), cloud cover (CLDTOT), solar radiation (SWGDN), 2m temperature (T2M), 10m U wind (U10M), 10m V wind (V10M), total precipitation (PRECTOT) and relative humidity (RH). These variables are 1-hour averages except for RH that is 3-hour averages. The hourly data is averaged into daily means for further analysis.

2.2. WPSH index and composite analysis

We first used the long-term ERA5 reanalysis SLP data (Hersbach et al., 2019; https://cds.climate.copernicus.eu/) to determine the climatology and variability to SLP over the northwestern Pacific. Figure 1a shows the multi-year averaged summertime SLP field from 1979 to 2018, and Figure 1b shows its standard deviation. Although the center of the high-pressure system is located over the Northeastern Pacific Ocean, it also shows substantial variability over the West Pacific extending to the east coast of China. This west branch has a significant impact on the summer weather patterns over Eastern China. Wang et al. (2013) defined a WPSH index to characterize the change of WPSH intensity. It is calculated as the mean of 850hPa geopotential height anomaly within the 15-25°N and 115-150°E region (red box in Figure 1b), where the maximum interannual variability of WPSH in the Western Pacific Ocean is located. Here we adopted the same method to calculate the geopotential height anomaly and divided the anomaly time series according to its standard deviation to obtain a normalized WPSH index. Then we used this index to represent the strength and variability of the WPSH (Figure 1c).

Using this WPSH index, we defined three types of WPSH conditions, namely strong, normal, and weak. Specifically, days with WPSH-index exceeding the 90^{th} percentile of its distribution are classified as strong WPSH days, the 45^{th} -55^{th} percentile as normal WPSH days, and those below the 10^{th} percentile as weak WPSH days (Figure 1c). There are two main reasons for the setting of this division standard: 1) using the 10% percentile range ensures that we have the same number of days during the summer from 2014 to 2018 for each type and enough sample (46 days for each type) for the composite analysis and statistical test; 2) the chosen of the percentile threshold is to maximize the difference between strong, weak and normal WPSH conditions in the time span of our study.

Composite analysis of observed and simulated surface ozone, meteorological variable as well as related model processes are performed based on these three types. We first calculate the composite mean of each variable for the 46 days of each WPSH type. As we focus on the ozone and meteorology differences induced by WPSH variation, we further calculated and discussed the difference of the composite mean between strong and normal WPSH as well as between weak and normal WPSH. The statistical significance of the difference is tested using the Student's-*t* test. We consider that the two composite means are statistically different if the test result is significant above 95% level. All figures except Figure 1 are displayed in the form of the differences between composite means.

2.3. GEOS-Chem simulations

We use the GEOS-Chem chemical transport model (CTM) (Bey et al., 2001; v12.3.2; http://geos-chem.org) to verify the responses of surface ozone in Eastern China to changes of the WPSH and to examine changes in the processes involved. GEOS-Chem includes a detailed O_x-NO_x-HC-aerosol-Br mechanism to describe gas and aerosol chemistry (Parella et al., 2012; Mao et al., 2013). The chemical mechanism follows the recommendations by the Jet Propulsion Laboratory (JPL) and the International Union of Pure and Applied Chemistry (IUPAC) (Sander, et al., 2011; IUPAC, 2013). Photolysis rates for tropospheric chemistry are calculated by the Fast-JX scheme (Bian and Prather (2002); Mao et al. (2010)). Transport is computed by the TPCORE advection algorithm of Lin and Rood (1996) with the archived GEOS meteorological data. Vertical transport due to convective transport is computed from the convective mass fluxes in the meteorological archive as described by Wu et al. (2007). As for boundary layer mixing, we used the non-local scheme implemented by Lin and McElroy (2010).

Emissions are configured using the Harvard-NASA Emission Component (HEMCO) (Keller et al., 2014). Biogenic VOC emissions, including isoprene, monoterpenes, and sesquiterpenes, are calculated online using the Model of Emissions of Gases and Aerosols from Nature (MEGAN v2.1, Guenther et al., 2012). Soil NOx emissions are calculated based on available nitrogen (N) in soils and edaphic conditions such as soil temperature and moisture (Hudman et al., 2012).

The model is driven by GEOS-FP meteorology fields and runs with 47 vertical levels and 2°× 2.5° horizontal resolution. The model simulations started from January 1st and ended on August 31st for each year during 2014 to 2018, in which the first five months were used as spin-up and June-July-August (JJA) are used for composite analysis. Anthropogenic emissions were fixed in 2010, after which the MIX emission inventory stopped updating, so that the differences among the three types of WPSH are solely caused by the change of meteorology. Because meteorology not only affects the production and transport of ozone but also significantly impacts the emission of BVOCs and NO_x from the soil, two important precursors of ozone formation. We also performed another set of simulations with MEGAN and soil NOx emissions turned off to explore the contribution of natural emissions; in this case, these two emission datasets are not read in during the simulation. We used ozone levels at the lowest model level with an average height of 58 m to represent model simulated surface ozone concentration.

2.4. Ozone Budget diagnosis

The simulated ozone concentration is determined by four processes, namely chemistry, transport (the sum of horizontal and vertical advection), mixing, and convection. Dry deposition is not separately discussed in the budget diagnosis, as this process is included in mixing when using the non-local PBL mixing scheme. However, as it is an important process for ozone removal, we show the dry deposition flux and velocity at the surface level in the supplementary (Figure S2). It is found that dry deposition velocity appears spatially correlated with precipitation, i.e., higher precipitation generally corresponds to higher dry deposition velocity, whereas dry deposition flux is proportional to the change in ozone concentrations (Figure 2). Budget diagnosis is further performed to quantify their individual contributions. The GEOS-Chem v12.1.0 or later versions provide budget diagnostics defined as the mass tendencies per grid cell (kg s^{-1}) for each species in the column (full, troposphere, or PBL) related to each GEOS-Chem component (e.g, chemistry). These diagnostics are calculated by taking the difference in the vertically integrated column ozone mass before and after chemistry, transport, mixing, and convection component in GEOS-Chem. Here we use the budget diagnostics in the PBL column and calculated composite means for each type of WPSH.

Regarding the region definition in this study, because in section 3.1 and section 3.2 the calculations are all site-based (city-average), we applied a single latitude division line of 32°N to separate Northern and Southern China and a longitude division line of 100°E as a boundary for a rough definition of Eastern China (green lines in Figure 2a). In section 3.3 and later, the paper mainly focused on the model result analysis, which is gird-based (region-average); thus, we used a north region and a south region with the same size and shape to ensure their comparability. The principle we chose the north and south region is based on the principle of avoiding the influence of coastline and covering as much land area as possible.

3. Results

3.1. Observed surface ozone changes associated with WPSH intensity

We first examine the relationship between observed MDA8 and WPSH-index of all cities in China. Figure 2a&b (symbols) respectively shows the difference in the composite mean of observed MDA8 between strong/weak WPSH days and normal WPSH days. A distinct dipole-like pattern can be observed in Figure 2a, indicating that during strong WPSH events, surface ozone concentration tends to be higher in Northern China but lower in Southern China, especially the southeast region. The transition from positive to negative changes happens around 32°N (Figure 2a), which is then used as the division between Northern and Southern China in this study. In contrast, Figure 2b, which shows the composite mean difference between weak and normal WPSH days, also exhibits a dipole pattern but opposite in sign to that shown in Figure 2a. Quantitatively, 45% and 31% of the cities show significant differences (p-value<0.05) in Student's t-test for the strong and weak WPSH relative to normal days, respectively. During strong WPSH days, the average MDA8 increased by 10.7 ppbv (+19%, Figure 2a&c) in Northern China and decreased by 11.2 ppbv (-24%, Figure 2a&c) in Southern China. Under weak WPSH conditions, the average MDA8 decreased by 10.2 ppbv (-17%, Figure 2b&d) in Northern China and increased by 4.6 ppbv (+10%, Figure 2b&d) in Southern China. This dipole change of ozone is also confirmed by a regression analysis of surface ozone against the WPSH index (Figure 2e), in which 71% cities show significant signals (p-value<0.05) with positive coefficients over Northern China and negative values in Southern China.

Composite and regression analysis jointly prove the robustness of the dipole-like ozone anomaly pattern associated with WPSH variability. It is likely that these changes are driven by changes in meteorological conditions. Therefore, in Figure 3, we further examine the differences of major meteorological variables associated with WPSH intensity.

The change of SLP associated with strong WPSH days clearly shows a positive center in the Northwest Pacific Ocean and to the east of China coast (Figure 3a). This high-pressure center induces anti-cyclonic circulation anomalies, which manifest themselves as southwest wind (10 m) anomalies over Eastern China (Figure 3a). In Northern China, because the surface winds are blown from the land area in the south (Figure 3a), it contains less moisture but with higher temperatures. As a result, Northern China exhibits a decrease in relative humidity (Figure 3e) and an increase in temperature (Figure 3k). Although the precipitation does not show significant changes, the decrease in cloud cover (Figure 3g) increases the near-surface solar radiation (Figure 3i) and can further change the photochemical reaction rates, which partly explains the increase of ozone concentrations here (Jeong and Park, 2013; Gong and Liao, 2019). The air stagnation associated with higher temperatures and less precipitation may also limit the diffusion and removal of ozone (Lu et al., 2019b; Pu et al., 2017). Moreover, previous studies showed that ozone is negatively correlated with precipitation and RH (Jeong and Park, 2013; Zhang et al., 2015). Among these meteorological variables, RH, solar radiation, temperature, and meridional wind are most closely related to surface ozone concentrations (Figure S3). In particular, for Northern China, the highest correlation (positive) is found between ozone and temperature. For Central Southern China along the Yangtze River basin, ozone is most highly correlated with RH. Whereas for

Southern China, wind speed and meridional winds seem to play the dominant role. The latter variable also shows a reversed relationship with ozone for Northern (positive) and Southern China (negative), highlighting the different characteristics in regional transport of ozone pollution. The results of our correlation analysis are also consistent with previous studies (Jeong and Park, 2013; Zhang et al., 2015; Gong and Liao, 2019). The overall changes of the meteorological fields in Northern China thus act to enhance surface ozone.

In Southern China, the south winds bring moisture from the ocean surface, providing ample water vapor for the rain band that forms on the northern boundary of the WPSH (Sampe et al., 2010; Rodriguez et al., 2019). This results in increased precipitation (Figure 3c), relative humidity (Figure 3e), and cloud cover (Figure 3g), and reduced surface shortwave radiation (Figure 3i). The increased precipitation and decreased solar radiation also help to lower the surface temperature (Figure 3k). The corresponding ozone concentration change is thus negative and opposite to that in Northern China. In addition, the transport of ozone-depleted air from the ocean can also dilute surface ozone.

Under the weak WPSH condition, it shows a negative anomaly center in the Northwest Pacific Ocean and to the southeast of China coast (Figure 3b). The changes of meteorological variables mostly show reversed patterns to those under strong WPSH cases, but some asymmetric features are noticed. For example, solar radiation decreased and total precipitation increased in Guangdong province, contrary to the general solar radiation enhancement and precipitation reduction in Southern China. However, these asymmetric changes in meteorology well match the observed decrease in ozone in Guangdong province.

According to the weather anomalies related to WPSH intensity, we summarize two pathways for ozone changes: (1) the relative changes of solar radiation and the associated meteorological variables impacting on the chemical formation of ozone; (2) the transport indicated by wind anomalies serves to enrich or dilute ozone concentration depending on the wind direction. Take Southern China as an example, the anticyclonic wind anomalies under strong WPSH tend to dilute ozone and the cyclonic wind anomalies under weak WPSH tend to enrich ozone, which is also confirmed in the budget analysis in section 3.4 below. Alternatively, this wind anomaly pattern drives an opposite change in ozone pollution over Northern China.

3.2. Simulated WPSH impacts on ozone air quality

Statistical analysis in Section 3.1 only reveals correlation but not causality. To investigate whether or not the WPSH-related meteorology changes indeed induce the dipole-like ozone change pattern, we perform GEOS-Chem simulations from 2014 to 2018 with anthropogenic emissions fixed in 2010. In this way, the model responses are purely attributed to changes in meteorology.

The model's capability in capturing ozone MDA8 concentrations in China is first evaluated by comparing the simulation results from 2014 to 2018 over all Chinese cities with observation (Figure S4). GEOS-Chem reproduces the observed seasonal spatial distributions of MDA8 reasonably well. The spatial correlation coefficients (R) between the observed and simulated seasonal mean MDA8 concentrations for summers from 2014 to 2018 are 0.57, 0.59, 0.70, 0.81, and 0.81, respectively. The mean bias (normalized mean bias) between the observed and simulated seasonal mean MDA8 concentrations are in the range of 7.1-9.4 ppbv (13%-22%) for summers from 2014 to 2018 (Figure S5). These evaluation results are comparable to those reported in previous studies (Lu et al., 2019b; Ni et al., 2018), despite the slight differences due to differences in season and sampling, proving the confidence of using GEOS-Chem to simulate ozone concentrations.

Figure 2 (filled contours) shows the simulated MDA8 changes during strong/weak WPSH days with respect to normal days (a&b) and their relative changes (c&d). The simulated strong/normal/weak values were calculated from the same days as the observations. Compared with observed changes (symbols), GEOS-Chem model well reproduces the dipole-like pattern of ozone change, albeit with a slight underestimation especially in Northern China. By calculating the average changes of simulated ozone concentration sampled at each city, we find the ozone responses to strong and weak WPSH are quite symmetric, with the average MDA8 increased by 3.6 ppbv (+6%) in

Northern China and decreased by 7.1 ppbv (-12%) in Southern China during strong WPSH (Figure 2a), and the average MDA8 decreased by 3.6 ppbv (-6%) in Northern China and increased by 6.6 ppbv (+11%) in Southern China during weak WPSH (Figure 2b). Although the WPSH index exhibits an asymmetric feature, with the difference between weak and normal days much larger than that between strong and normal days, the responses of meteorological variables appear more symmetric (Figure 3). This thus leads to a more symmetric change in ozone concentrations (Figure 2). Therefore, we consider this asymmetric behavior in WPSH strength has a negligible effect in the response of ozone pollution. The slight underestimation of model results compared with observation may come from the model's lack of ability in capturing the peak values of ozone MDA8 (Zhang and Wang, 2016; Ni et al., 2018).

3.3 Budget diagnosis

In order to examine and to quantify the chemical and physical processes that lead to the ozone change, Figure 4 provides the budget diagnostics of chemistry, transport, mixing, and convection in the PBL column. Chemistry represents the changes in net chemical production, which is determined by the change of reaction rate and the amount of ozone precursors. As the photolysis rate and natural precursor emissions are both influenced by meteorological conditions, the change of chemical production is consistent with the variation of solar radiation and temperature in Figure 3. Under the strong WPSH condition, ozone concentrations from chemical production exhibit a tripolar structure, with increases in Northern China and the southern edge and decreases in the Yangtze River basin (Figure 4a).

Transport represents the change of horizontal and vertical advection of ozone. For strong WPSH, the ozone budget due to the transport budget exhibits an asymmetric pattern with decreases in most parts of Southern China and increases over Northern and Northeastern China (Figure 4c). As the correlation analysis shows that ozone responds to meridional wind positively in the north and negatively in the south (Figure S3i), the changes in transport budget are consistent with the WPSH-induced wind anomalies (Figure 3a), which tends to dilute surface ozone in the south and enhance it in the north. The mixing process describes turbulence diffusion in the boundary layer. Mixing in the whole PBL column represents the total exchange of PBL with the free troposphere, which shows a roughly reversed pattern to chemistry (Figure 4e). Cloud convection shows a general dipole pattern with positive signals in the north and negative signals in the south. However, the small changes in the absolute value suggest a weak impact via deep convection (Figure 4g). Under weak WPSH conditions, ozone from chemical production significantly increases in the east of Southern China but decreases strongly in Northern and Southwestern China (Figure 4b). According to the wind anomalies in Figure 3b, transport tends to minimize the difference induced by chemistry and thus leads to an opposite ozone change (Figure 4d). Mixing shows a distinct north-south contrast pattern (Figure 4f). Convection changes slightly in opposite direction in the north and south (Figure 4h). Due to PBL mixing, the total change of these processes

(Figure 4i&j) in the PBL column shows a consistent pattern with both the observed and simulated change of surface ozone (Figure 2). In general, chemistry (Figure 4a&b) and transport (Figure 4c&d) account for the largest proportions of ozone change than the other two mechanisms (i.e., mixing, Figure 4e&f, and convection, Figure 4g&h).

In order to provide a more quantitative evaluation of the contribution of these processes, in Figure 4k-n, we examine the regionally averaged ozone changes for a North (36.0-42.0°N, 105.0-117.5°E) and South (26.0-32.0°N, 107.5-120.0°E) region, respectively defined by the purple and black boxes on Figure 4i&j. It can be seen that the regionally averaged total ozone change is around $\pm$1-2 kg s^{-1}. In all cases except Northern China under strong WPSH, chemistry appears to be the dominating process, which results in the largest ozone change and with the same sign as the total change and sometimes can even exceed the amount of total change. For the Northern China case, transport slightly outweighs chemistry as the primary factor (Figure 4k). Transport contributes to total changes either positively or negatively, depending on the ozone concentration gradient and wind anomalies. It tends to increase ozone when the wind anomalies come from inland regardless of the direction (Figure 4k&m&n). In contrast, when the wind comes from the ocean, it serves to reduce surface ozone (Figure 4l). As the mixing process transports ozone along the vertical concentration gradient, it generally contributes negatively to the total ozone change and thus counteracts excessive chemical changes (Figure 4l-n). Convection only induces minor modulation to the total changes, generally less than $\pm$1 kg s^{-1} and negligible for some cases (Figure 4l&m). There are two possible reasons for this insignificant change. On the one hand, as ozone is insoluble in water, the large changes in convective activities associated with the WPSH variation may only exert minor effect on the ozone concentration through wet scavenging. Instead, it influences ozone concentration by the vertical transport of ozone as well as its precursors, but the average change of ozone budget due to convection transport is about an order of magnitude smaller than that due to chemical processes. On the other hand, previous studies show that the effect of convective transport of ozone alone is to reduce the tropospheric column amounts while the convective transport of the ozone precursors tends to overcome this reduction (Wu et al., 2007; Lawrence et al., 2003). As a result, changes in ozone are neutralized and the net effect is weak.

3.4 The contribution of natural emission of ozone precursor gases

In the GEOS-Chem simulation, all anthropogenic emissions are fixed, so there is no anthropogenic contribution to the simulated ozone change. However, the emission of ozone precursor gases from natural sources, primarily biogenic volatile organic compounds (BVOCs) and soil-released NOx (SNOx), closely respond to meteorology and further impact the chemical production of ozone, which has been identified as the main driving force of ozone change (see Section 3.3). Therefore, in this section, we continue to quantify the contribution of BVOCs and soil NOx emission to the ozone changes with WPSH.

Isoprene (used as a proxy of BVOCs) emissions are strongly correlated with temperatures and increase rapidly between 15 and 35 °C (Fehsenfeld et al., 1992; Guenther et al., 1993); thus, the pattern of their changes with WPSH are highly consistent with the T2 changes (Figure 5a&b). Intensified WPSH results in 10-40% increases of BVOCs emissions in Northern China and 10-30% decreases in Southern China, whereas under weak WPSH conditions, they increase strongly in most parts of China but with a slight decrease over the Northern China Plain and Northeastern China. Changes in NOx emission from the soil also exhibit a similar pattern to those of T2. Their responses to weak WPSH appear to be stronger than BVOCs, with decreases up to 40% over most of Northern China (Figure 5c&d). As most parts of China are the high-NOx and VOC-limited regions, the overall decreases of BVOCs and NOx reduce the ozone concentration.

We further quantify the contribution of BVOCs and soil NOx emissions to the changes in surface ozone concentration by comparing simulation results with MEGAN and soil emissions turned on and off. Figure 6a&b and 6c&d show the simulated MDA8 ozone with biogenic and soil NOx emissions on and off, respectively. They show similar spatial patterns but the emission-off case exhibits weaker responses. Figure 6e&f shows their differences, which represent the MDA8 changes due to the combined effect of BVOCs and soil NOx emission changes associated with WPSH variation. The precursor-induced ozone changes are in phase with the total ozone changes in most parts of China and show a dipole-like pattern. In total, these two factors result in ~±1.3 ppbv MDA8 ozone changes (averaged over all cities), which accounts for around 30% of the total simulated change. Figure6 g&h and i&j show the contribution of soil NOx and BVOCs emissions, respectively, from which we can see that the ozone change induced by soil NO_x is weaker, implying that BVOCs is the dominant factor. Figure 6k-n shows the averaged contributions from individual and total emissions of BVOCs and soil NOx for a north and south region marked respectively by purple and black boxes in Figure 6a&b. The averaged ozone changes in the North and South region are in the range of -4~4 ppbv, and BVOCs and soil NOx on average contribute 28% to the total changes. The combined contribution of BVOCs and soil NOx is more consistent with that of BVOCs, and the soil NOx-induced changes are small in all cases except Northern China under the weak WPSH conditions. The exception in Figure 6m might be due to the ratio of VOC to NOx in the North region under weak WPSH conditions, which shifts towards the NOx-limited regime, making ozone concentration more sensitive to the change of NOx. In sum, the result emphasizes the role of BVOCs emission in total chemistry production.

4. Conclusions and Discussion

In this study, we highlight the role of weather systems like WPSH on surface ozone pollution in China interpreted with a comprehensive mechanism analysis. Statistical analysis of surface observation reveals a dipole-like ozone change associated with the WPSH intensity, with stronger WPSH increasing surface ozone concentration over Northern China but reducing it over Southern China, and a reversed pattern during its weak phase. This phenomenon is associated with the change of meteorological conditions induced by the change of WPSH intensity. Specifically, when WPSH is stronger than normal, dry, hot south winds from inland area serves to increase temperature in Northern China but decrease relative humidity, cloud cover, and precipitation, creating an environment that is favorable for surface ozone formation. In Southern China, the changes of meteorology and ozone are reversely symmetric to the north. Opposite changes are found during weaker WPSH conditions.

This dipole pattern of surface ozone changes is well reproduced by the GEOS-Chem model simulations, which not only confirms the impact of meteorology on ozone concentration, but also allows the diagnosis of the processes involved in ozone change, namely chemistry, transport, mixing, and convection processes. Our results show that chemistry and transport processes play more important roles than mixing and convection. The transport budget confirms the pattern and quantifies the magnitude of regional transport indicated by the wind anomalies in the meteorological fields. The enormous change in the chemistry budget shows that chemical production serves as the leading process determining the direction of the ozone change. As the anthropogenic emission is fixed, the chemistry process is influenced by the changes in natural emission and chemical reaction rates associated with WPSH variations. By comparing the

GEOS-Chem simulations with the MEGAN and soil emissions turned on and off, we determined that ozone changes caused by natural emissions (including BVOCs and soil NO_x) account for ~30% of the total ozone changes. The GEOS-Chem simulations in our study serve as a useful tool to provide more quantitative insights and analysis, which compensate for the statistical analysis results in previous studies (Zhao and Wang, 2017; Yin et al., 2019).

As WPSH is associated with continental-scale circulation patterns, such as the East Asian Summer Monsoon (EASM), several previous studies also discussed the impact of EASM on ozone pollution in China (Yang et al., 2014; Han et al., 2020). However, our study differs from the EASM related ones in that (1) the EASM has complex space and time structures that encompass tropics, subtropics, and midlatitudes. Given its complexity, it is difficult to use a simple index to represent the variability of EASM (Wang et al., 2008; Ye et al., 2019), whereas the location and definition for WPSH are more definitive (Lu et al., 2002; Wang et al., 2012); and (2) The influences of EASM on ozone mainly represent interannual scale as EASM indices are defined by month/year, while the WPSH is a system more suitable to explore the day to day variability ozone, which is meaningful for short-term ozone air quality prediction.

A better understanding of the internal mechanism of WPSH's impact on ozone air quality can also help assess the air quality variation more comprehensively under climate change. The location and intensity of WPSH keep changing over time, e.g., Zhou et al. (2009) demonstrated that WPSH had extended westward since the late 1970s, and Li et al. (2012) indicated that North Pacific Subtropical High would intensify in the twenty-first century as climate warms. Nonetheless, there still exists a great uncertainty about how WPSH will change under climate change, and further studies are needed to discuss the responses of ozone to synoptic weather systems like WPSH in future scenarios. In addition, the variability of WPSH is found to be related to global climate variabilities such as ENSO (Paek et al., 2019) and PDO (Matsumura et al., 2016). Therefore, how natural climate variabilities like ENSO and PDO interact with WPSH to impact ozone air quality also needs more investigation.

Data and model availability

All the measurements, meteorological data are accessible online through the websites given above. The GEOS-Chem model is a community model and is freely available (www.geos-chem.org).

Author contributions

J.L. and Z.J. designed the study. Z.J. ran the GEOS-Chem model and performed the analysis. X.L. and L.Z. helped in the GEOS-Chem simulation. C.G. and H.L. helped in the budget diagnosis. Z.J. and J.L. wrote the paper. All authors contributed to the interpretation of results and the improvement of this paper.

Competing interests

The authors declare that they have no conflict of interest.

Acknowledgement

We thank the China National Environmental Monitoring Centre for supporting the nationwide ozone monitoring network and the website (http://beijingair.sinaapp.com/) for collecting and sharing hourly ozone concentration data. We appreciate GMAO for providing the GEOS-FP meteorological data (http://ftp.as.harvard.edu/gcgrid/data/GEOS_2x2.5/GEOS_FP). We thank EMWCF for providing the ERA5 reanalysis data (https://cds.climate.copernicus.eu/). We also acknowledge the efforts of GEOS-Chem Working Groups and Support Team for developing and maintaining the GEOS-Chem model.

Financial Support

This work is funded by the National Key Research and Development Program of China (No. 2017YFC0212803) and Open fund by Jiangsu Key Laboratory of Atmospheric Environment Monitoring and Pollution Control (KHK1901).

References

Bey, I., Jacob, D. J., Yantosca, R. M., Logan, J. A., Field, B. D., Fiore, A. M., Li, Q., Liu, H. Y., Mickley, L. J., and Schultz, M. G.: Global modeling of tropospheric chemistry with assimilated meteorology: Model description and evaluation, J. Geophys. Res., 106, 23073-23095, https://doi.org/10.1029/2001JD000807, 2001.

Bian, H. S., and Prather, M. J.: Fast-J2: Accurate simulation of stratospheric photolysis in global chemical models, J. Atmos. Chem., 41, 281-296, https://doi.org/10.1023/a:1014980619462, 2002.

Choi, W., and Kim, K.-Y.: Summertime variability of the western North Pacific subtropical high and its synoptic influences on the East Asian weather, Sci. Rep., 9, https://doi.org/10.1038/s41598-019-44414-w, 2019.

Fehsenfeld, F., Calvert, J., Fall, R., Goldan, P., Guenther, A., Hewitt, C., Lamb, B., Liu, S., Trainer, M., Westberg, H., and Zimmerman, P.: Emissions of volatile organic compounds from vegetation and the implications for atmospheric chemistry, Global Biogeochem. Cycles, 6, 389-430, https://doi.org/10.1029/92gb02125, 1992.

Fleming, Z. L., Doherty, R. M., Von Schneidemesser, E., Malley, C. S., Cooper, O. R., Pinto, J. P., Colette, A., Xu, X., Simpson, D., Schultz, M. G., Lefohn, A. S., Hamad, S., Moolla, R., Solberg, S. and Feng, Z.: Tropospheric Ozone Assessment Report: Present-day ozone distribution and trends relevant to human health, Elem. Sci. Anth., 6:12. https://doi.org/10.1525/elementa.273, 2018.

Gao, H., Jiang, W., and Li, W.: Changed Relationships Between the East Asian Summer Monsoon Circulations and the Summer Rainfall in Eastern China, J. Meteorolog. Res., 28, 1075-1084, https://doi.org/10.1007/s13351-014-4327-5, 2014.

Gong, C., and Liao, H.: A typical weather pattern for ozone pollution events in North China, Atmos. Chem. Phys., 19, 13725-13740, https://doi.org/10.5194/acp-19-13725-2019, 2019.

Guenther, A. B., Zimmerman, P. R., Harley, P. C., Monson, R. K., and Fall, R.: Isoprene and monoterpene emission rate variability, Model evaluations and sensitivity analyses, J. Geophys. Res., 98, 12609-12617, https://doi.org/10.1029/93jd00527, 1993.

Guenther, A. B., Jiang, X., Heald, C. L., Sakulyanontvittaya, T., Duhl, T., Emmons, L. K., and Wang, X.: The Model of Emissions of Gases and Aerosols from Nature version 2.1 (MEGAN2.1): an extended and updated framework for modeling biogenic emissions, Geosci. Model Dev., 5, 1471–1492, https://doi.org/10.5194/gmd-5- 1471-2012, 2012.

Han, H., Liu, J., Shu, L., Wang, T., and Yuan, H.: Local and synoptic meteorological influences on daily variability in summertime surface ozone in eastern China, Atmos. Chem. Phys., 20, 203-222, https://doi.org/10.5194/acp-20-203-2020, 2020.

Heck, W. W., Adams, R. M., Cure, W. W., Heagle, A. S., Heggestad, H. E., Kohut, R. J., Kress, L. W., Rawlings, J. O., and Taylor, O. C.: A reassessment of crop loss from ozone, Environ. Sci. Technol., 17, A572-A581, https://doi.org/10.1021/es00118a001, 1983.

Hersbach, H., Bell, B., Berrisford, P., Biavati, G., Horányi, A., Muñoz Sabater, J., Nicolas, J., Peubey, C., Radu, R., Rozum, I., Schepers, D., Simmons, A., Soci, C., Dee, D., Thépaut, J-N. (2019): ERA5 monthly averaged data on single levels from 1979 to present. Copernicus Climate Change Service (C3S) Climate Data Store (CDS). (Accessed on < 29-DEC-2020 >), 10.24381/cds.f17050d7.

Hoesly, R. M., Smith, S. J., Feng, L., Klimont, Z., Janssens-Maenhout, G., Pitkanen, T., Seibert, J. J., Linh, V., Andres, R. J., Bolt, R. M., Bond, T. C., Dawidowski, L., Kholod, N., Kurokawa, J.-i., Li, M., Liu, L., Lu, Z., Moura, M. C. P., O'Rourke, P. R., and Zhang, Q.: Historical (1750-2014) anthropogenic emissions of reactive gases and aerosols from the Community Emissions Data System (CEDS), Geosci. Model Dev., 11, 369-408, https://doi.org/10.5194/gmd-11-369-2018, 2018.

Huang, Y., Wang, B., Li, X., and Wang, H.: Changes in the influence of the western Pacific subtropical high on Asian summer monsoon rainfall in the late 1990s, Clim. Dyn., 51, 443-455, https://doi.org/10.1007/s00382-017-3933-1, 2018.

Hudman, R. C., Moore, N. E., Mebust, A. K., Martin, R. V., Russell, A. R., Valin, L. C., and Cohen, R. C.: Steps towards a mechanistic model of global soil nitric oxide emissions: implementation and space based-constraints, Atmos. Chem. Phys., 12, 7779–7795, https://doi.org/10.5194/acp-12-7779-2012, 2012.

IUPAC: Task group on atmospheric chemical kinetic data evaluation by International Union of Pure and Applied Chemistry (IUPAC), available at: http://iupac.pole-ether.fr/ (last access: 12th May 2020), 2013.

Jacob, D. J., and Winner, D. A.: Effect of climate change on air quality, Atmos. Environ., 43, 51-63, https://doi.org/10.1016/j.atmosenv.2008.09.051, 2009.

Jeong, J. I. and Park, R. J.: Effects of the meteorological variability on regional air quality in East Asia, Atmos. Environ., 69, 46–55, https://doi.org/10.1016/j.atmosenv.2012.11.061, 2013.

Keller, C. A., Long, M. S., Yantosca, R. M., Da Silva, A. M., Pawson, S., and Jacob, D. J.: HEMCO v1.0: a versatile, ESMF-compliant component for calculating emissions in atmospheric models, Geosci. Model Dev., 7, 1409–1417, https://doi.org/10.5194/gmd-7-1409-2014, 2014.

Kuhns, H., Knipping, E. M., and Vukovich, J. M.: Development of a United States–Mexico Emissions Inventory for the Big Bend Regional Aerosol and Visibility Observational (BRAVO) Study, J. Air Waste Manage. Assoc., 55, 677-692, https://doi.org/10.1080/10473289.2005.10464648, 2005.

Li, K., Jacob, D. J., Liao, H., Shen, L., Zhang, Q., and Bates, K. H.: Anthropogenic drivers of 2013-2017 trends in summer surface ozone in China, PNAS, 116, 422-427, https://doi.org/10.1073/pnas.1812168116, 2019.

Li, M., Zhang, Q., Kurokawa, J.-i., Woo, J.-H., He, K., Lu, Z., Ohara, T., Song, Y., Streets, D. G., Carmichael, G. R., Cheng, Y., Hong, C., Huo, H., Jiang, X., Kang, S., Liu, F., Su, H., and Zheng, B.: MIX: a mosaic Asian anthropogenic emission inventory under the international collaboration framework of the MICS-Asia and HTAP, Atmos. Chem. Phys., 17, 935-963, https://doi.org/10.5194/acp-17-935-2017, 2017a.

Li, W., Li, L., Ting, M., and Liu, Y.: Intensification of Northern Hemisphere subtropical highs in a warming climate, Nat. Geosci., 5, 830-834, https://doi.org/10.1038/ngeo1590, 2012.

Lin, J.-T., and M. McElroy, Impacts of boundary layer mixing on pollutant vertical profiles in the lower troposphere: Implications to satellite remote sensing, Atmos. Environ., 44(14), 1726-1739, https://doi.org/10.1016/j.atmosenv.2010.02.009, 2010.

Lin, S., and Rood, R. B.: Multidimensional Flux-Form Semi-Lagrangian Transport Schemes, Mon. Weather Rev., 124, 2046-2070, 10.1175/1520-0493(1996)124<2046:MFFSLT>2.0.CO;2, 1996.

Liu, H., Liu, S., Xue, B., Lv, Z., Meng, Z., Yang, X., Xue, T., Yu, Q., and He, K.: Ground-level ozone pollution and its health impacts in China, Atmos. Environ., 173, 223-230, https://doi.org/10.1016/j.atmosenv.2017.11.014, 2018.

Liu, J., Wang, L., Li, M., Liao, Z., Sun, Y., Song, T., Gao, W., Wang, Y., Li, Y., Ji, D., Hu, B., Kerminen, V.-M., Wang, Y., and Kulmala, M.: Quantifying the impact of synoptic circulation patterns on ozone variability in northern China from April to October 2013-2017, Atmos. Chem. Phys., 19, 14477-14492, https://doi.org/10.5194/acp-19-14477-2019, 2019.

Lu, R.: Indices of the summertime western North Pacific subtropical high, Adv. Atmos. Sci., 19, 1004-1028, https://doi.org/10.1007/s00376-002-0061-5, 2002.

Lu, X., Hong, J., Zhang, L., Cooper, O. R., Schultz, M. G., Xu, X., Wang, T., Gao, M., Zhao, Y., and Zhang, Y.: Severe Surface Ozone Pollution in China: A Global Perspective, Environ. Sci. Technol. Lett., 5, 487-494, https://doi.org/10.1021/acs.estlett.8b00366, 2018.

Lu, X., Zhang, L., and Shen, L.: Meteorology and Climate Influences on Tropospheric Ozone: a Review of Natural Sources, Chemistry, and Transport Patterns, Current Pollution Reports, 5, 238-260, https://doi.org/10.1007/s40726-019-00118-3, 2019a.

Lu, X., Zhang, L., Chen, Y., Zhou, M., Zheng, B., Li, K., Liu, Y., Lin, J., Fu, T.-M., and Zhang, Q.: Exploring 2016-2017 surface ozone pollution over China: source contributions and meteorological influences, Atmos. Chem. Phys., 19, 8339-8361, https://doi.org/10.5194/acp-19-8339-2019, 2019b.

Lu, X., Zhang, L., Wang, X., Gao, M., Li, K., Zhang, Y., Yue, X., and Zhang, Y.: Rapid increases in warm-season surface ozone and resulting health impact over China since 2013, Environ. Sci. Technol. Lett., https://doi.org/10.1021/acs.estlett.0c00171, 2020.

Lucchesi, R., 2013: File Specification for GEOS-5 FP. GMAO Office Note No. 4 (Version 1.0), 63 pp, available from http://gmao.gsfc.nasa.gov/pubs/office_notes.

Maji, K. J., Ye, W.-F., Arora, M., and Nagendra, S. M. S.: Ozone pollution in Chinese cities: Assessment of seasonal variation, health effects and economic burden, Environ. Pollut., 247, 792-801, https://doi.org/10.1016/j.envpol.2019.01.049, 2019.

Mao, J., Sun, Z., and Wu, G.: 20–50-day oscillation of summer Yangtze rainfall in response to intraseasonal variations in the subtropical high over the western North Pacific and South China Sea, Clim. Dyn., 34, 747-761, https://doi.org/10.1007/s00382-009-0628-2, 2010.

Mao, J., Paulot, F., Jacob, D. J., Cohen, R. C., Crounse, J. D., Wennberg, P. O., Keller, C. A., Hudman, R. C., Barkley, M. P., and Horowitz, L. W.: Ozone and organic nitrates over the eastern United States: Sensitivity to isoprene chemistry, J. Geophys. Res., 118, https://doi.org/10.1002/jgrd.50817, 2013.

Marais, E. A., and Wiedinmyer, C.: Air Quality Impact of Diffuse and Inefficient Combustion Emissions in Africa (DICE800 Africa), Environ. Sci. Technol., 50, 10739-10745, https://doi.org/10.1021/acs.est.6b02602, 2016.

Matsumura, S., and Horinouchi, T.: Pacific Ocean decadal forcing of long-term changes in the western Pacific subtropical high, Sci. Rep., 6, 37765, https://doi.org/10.1038/srep37765, 2016.

Mills G, Pleijel H, Malley CS, Sinha B, Cooper OR, Schultz MG, Neufeld HS, Simpson

D, Sharps K, Feng Z, Gerosa G, Harmens H, Kobayashi K, Saxena P, Paoletti E, Sinha V, Xu X., Tropospheric Ozone Assessment Report: Present-day tropospheric ozone distribution and trends relevant to vegetation. Elem. Sci. Anth., 6: 47. https://doi.org/10.1525/elementa.302, 2018.

Ministry of Environmental Protection of the People’s Republic of China, 2012. Ambient Air Quality Standards (GB3095-2012).

Ministry of Environmental Protection of the Peoples Republic of China, 2013. Specifications and Test Procedures from Ambient Air Quality Continuous Automated Monitoring System for SO2、NO2、O3 and CO (HJ 654-2013).

Monks, P. S., Archibald, A. T., Colette, A., Cooper, O. R., Coyle, M., Derwent, R. G., Fowler, D., Granier, C., Law, K. S., and Mills, G.: Tropospheric ozone and its precursors from the urban to the global scale from air quality to short-lived climate forcer, Atmos. Chem. Phys., 15, 8889-8973, https://doi.org/10.5194/acp-15-8889-2015, 2015.

Ni, R., Lin, J., Yan, Y., and Lin, W.: Foreign and domestic contributions to springtime ozone over China, Atmos. Chem. Phys., 18, 11447–11469, https://doi.org/10.5194/acp-18-11447-2018, 2018.

Paek, H., Yu, J.-Y., Zheng, F., and Lu, M.-M.: Impacts of ENSO diversity on the western Pacific and North Pacific subtropical highs during boreal summer, Clim. Dyn., 52, 7153-7172, https://doi.org/10.1007/s00382-016-3288-z, 2019.

Parrella, J. P., Jacob, D. J., Liang, Q., Zhang, Y., Mickley, L. J., Miller, B., Evans, M. J., Yang, X., Pyle, J. A., Theys, N., and Van Roozendael, M.: Tropospheric bromine chemistry: implications for present and pre-industrial ozone and mercury, Atmos. Chem. Phys., 12, 6723–6740, https://doi.org/10.5194/acp-12-6723-2012, 2012.

Pu, X., Wang, T. J., Huang, X., Melas, D., Zanis, P., Papanastasiou, D. K., and Poupkou, A.: Enhanced surface ozone during the heat wave of 2013 in Yangtze River Delta region, China, Sci. Total Environ., 603-604, 807-816, https://doi.org/10.1016/j.scitotenv.2017.03.056, 2017.

Rasmussen, D. J., Fiore, A. M., Naik, V., Horowitz, L. W., McGinnis, S. J., and Schultz, M. G.: Surface ozone-temperature relationships in the eastern US: A monthly climatology for evaluating chemistry-climate models, Atmos. Environ., 47, 142-153, https://doi.org/10.1016/j.atmosenv.2011.11.021, 2012.

Rodriguez, J. M., and Milton, S. F.: East Asian Summer Atmospheric Moisture Transport and Its Response to Interannual Variability of the West Pacific Subtropical High: An Evaluation of the Met Office Unified Model, Atmosphere, 10, https://doi.org/10.3390/atmos10080457, 2019.

Sampe, T., and Xie, S.-P.: Large-Scale Dynamics of the Meiyu-Baiu Rainband: Environmental Forcing by the Westerly Jet, J. Clim., 23, 113-134, https://doi.org/10.1175/2009jcli3128.1, 2010.

Sander, S. P., Golden, D., Kurylo, M., Moortgat, G.,Wine, P., Ravishankara, A., Kolb, C., Molina, M., Finlayson-Pitts, B., and Huie, R.: Chemical kinetics and photochemical data for use in atmospheric studies, JPL Publ., 06-2, 684 pp., 2011.

Silver, B., Reddington, C. L., Arnold, S. R., and Spracklen, D. V.: Substantial changes in air pollution across China during 2015–2017, Environ. Res. Lett., 13, 114012, https://doi.org/10.1088/1748-9326/aae718, 2018.

Shu, L., Xie, M., Wang, T., Gao, D., Chen, P., Han, Y., Li, S., Zhuang, B., and Li, M.: Integrated studies of a regional ozone pollution synthetically affected by subtropical high and typhoon system in the Yangtze River Delta region, China, Atmos. Chem. Phys., 16, 15801-15819, https://doi.org/10.5194/acp-16-15801-2016, 2016.

Tai, A. P. K., Martin, M. V., and Heald, C. L.: Threat to future global food security from climate change and ozone air pollution, Nat. Clim. Change, 4, 817-821, https://doi.org/10.1038/nclimate2317, 2014.

van der Werf, G. R., Randerson, J. T., Giglio, L., van Leeuwen, T. T., Chen, Y., Rogers, B. M., Mu, M., van Marle, M. J. E., Morton, D. C., Collatz, G. J., Yokelson, R. J., and Kasibhatla, P. S.: Global fire emissions estimates during 1997–2016, Earth Syst. Sci. Data, 9, 697–720, https://doi.org/10.5194/essd-9-697-2017, 2017.

Wang, B., Wu, Z., Li, J., Liu, J., Chang, C.-P., Ding, Y., and Wu, G.: How to Measure the Strength of the East Asian Summer Monsoon, J. Clim., 21, 4449-4463, https://doi.org/10.1175/2008jcli2183.1, 2008.

Wang, B., Xiang, B., and Lee, J.-Y.: Subtropical High predictability establishes a promising way for monsoon and tropical storm predictions, PNAS, 110, 2718-2722, https://doi.org/10.1073/pnas.1214626110, 2013.

Wang, T., Xue, L., Brimblecombe, P., Lam, Y. F., Li, L., and Zhang, L.: Ozone pollution in China: A review of concentrations, meteorological influences, chemical precursors, and effects, Sci. Total Environ., 575, 1582-1596, https://doi.org/10.1016/j.scitotenv.2016.10.081, 2017.

Wu, S., L.J. Mickley, D.J. Jacob, J.A. Logan, R.M. Yantosca, and D. Rind, Why are there large differences between models in global budgets of tropospheric ozone?, J. Geophys. Res., 112, D05302, https://doi.org/10.1029/2006JD007801, 2007.

Ye, M., and Chen, H.: Recognition of two dominant modes of EASM and its thermal driving factors based on 25 monsoon indexes, Atmos. Oceanic Sci. Lett., 12, 278-285, https://doi.org/10.1080/16742834.2019.1614424, 2019.

Yin, Z., Cao, B., and Wang, H.: Dominant patterns of summer ozone pollution in eastern China and associated atmospheric circulations, Atmos. Chem. Phys., 19, 13933–13943, https://doi.org/10.5194/acp-19-13933-2019, 2019.

Zhang, H., Wang, Y., Hu, J., Ying, Q., and Hu, X.-M.: Relationships between meteorological parameters and criteria air pollutants in three megacities in China, Environ. Res., 140, 242-254, https://doi.org/10.1016/j.envres.2015.04.004, 2015.

Zhang, Y. and Wang, Y.: Climate-driven ground-level ozone extreme in the fall over the Southeast United States, P. Natl. Acad. Sci. USA, 113, 10025–10030, https://doi.org/10.1073/pnas.1602563113, 2016.

Zhao, Z., and Wang, Y.: Influence of the West Pacific subtropical high on surface ozone daily variability in summertime over eastern China, Atmos. Environ., 170, 197-204, https://doi.org/10.1016/j.atmosenv.2017.09.024, 2017.

Zhou, T., Yu, R., Zhang, J., Drange, H., Cassou, C., Deser, C., Hodson, D. L. R., Sanchez-Gomez, E., Li, J., Keenlyside, N., Xin, X., and Okumura, Y.: Why the Western Pacific Subtropical High Has Extended Westward since the Late 1970s, J. Clim., 22, 2199-2215, https://doi.org/10.1175/2008jcli2527.1, 2009.

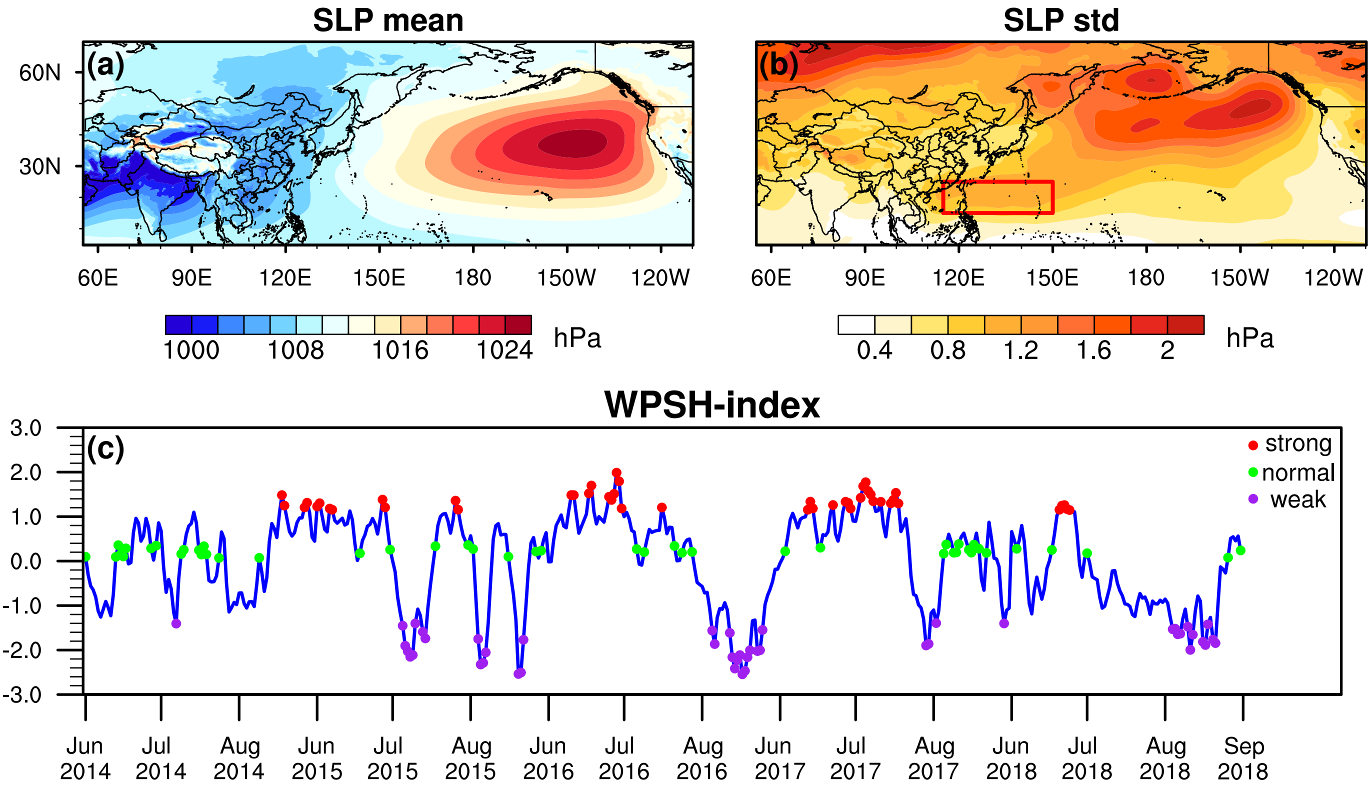

Figure 1. West Pacific Mean Sea Level Pressure (a) and its standard deviation (b), calculated using June, July, August (JJA) data from 1979 to 2018. Red box in (b) indicates the region (15-25°N, 115-150°E) used to calculate the WPSH-index. (c) shows the time series of WPSH-index and the selections of three types of WPSH. The blue line represents the normalized WPSH-index of 460 days in JJA from 2014 to 2018. Red dots represent strong WPSH days, green dots represent normal WPSH days and purple dots represent weak WPSH days.

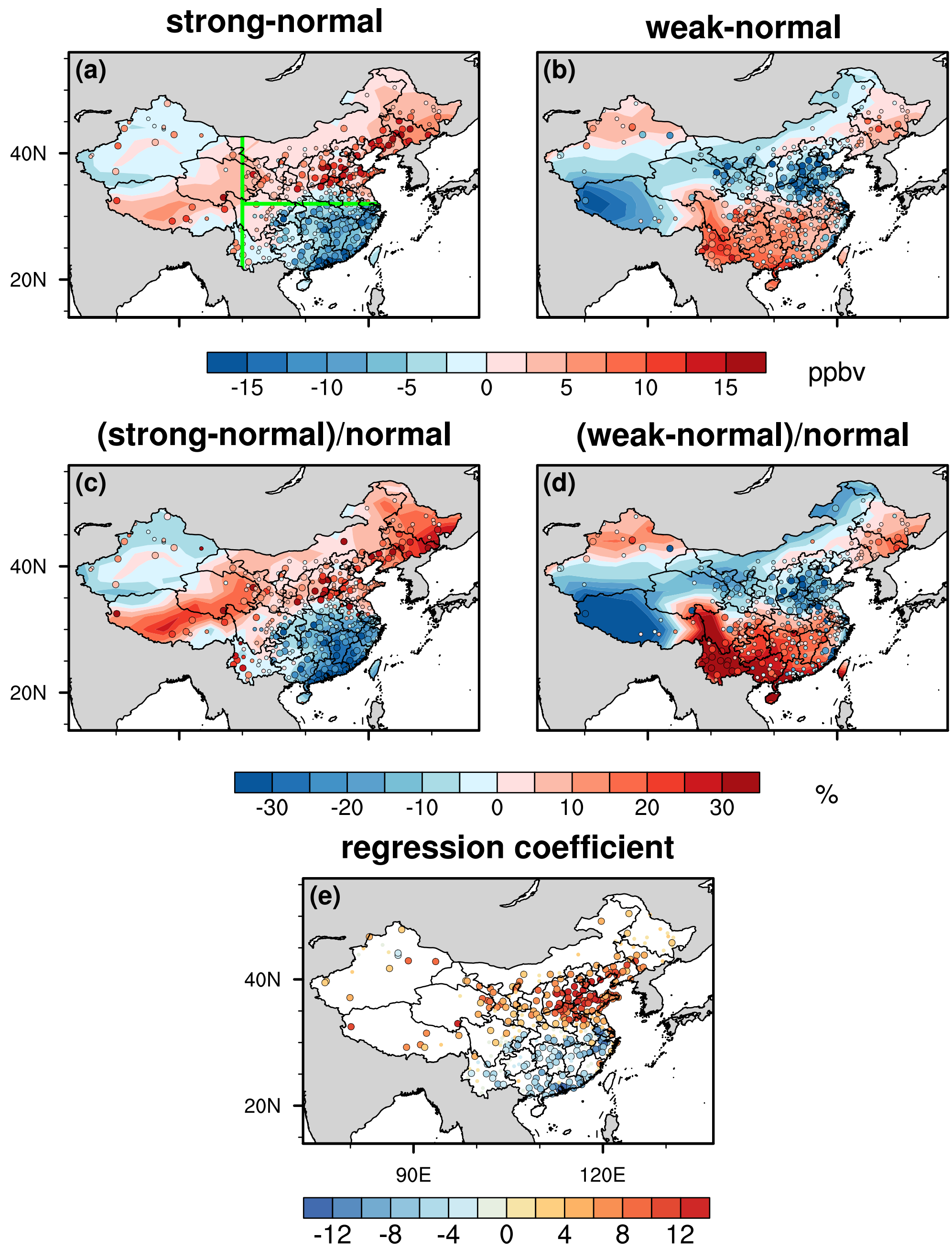

Figure 2. The observed (symbols) and simulated (filled contours) difference of MDA8 (ppbv) during strong and weak WPSH relative to normal WPSH days. (a) MDA8 of strong WPSH minus normal WPSH days, (b) MDA8 of weak WPSH minus normal WPSH days. (c) The percentage change of MDA8 of strong WPSH relative to normal, (d) the percentage change of MDA8 of weak WPSH relative to normal. (e) The regression coefficient between MDA8 in JJA from 2014 to 2018 and WPSH-index for cities in China. Larger dots with black circles in (a-e) are sites with significant level less than 0.05 from Student's t-test. The vertical green line in (a) is the boundary of Eastern China and the horizontal green line is the division of Northern and Southern China.

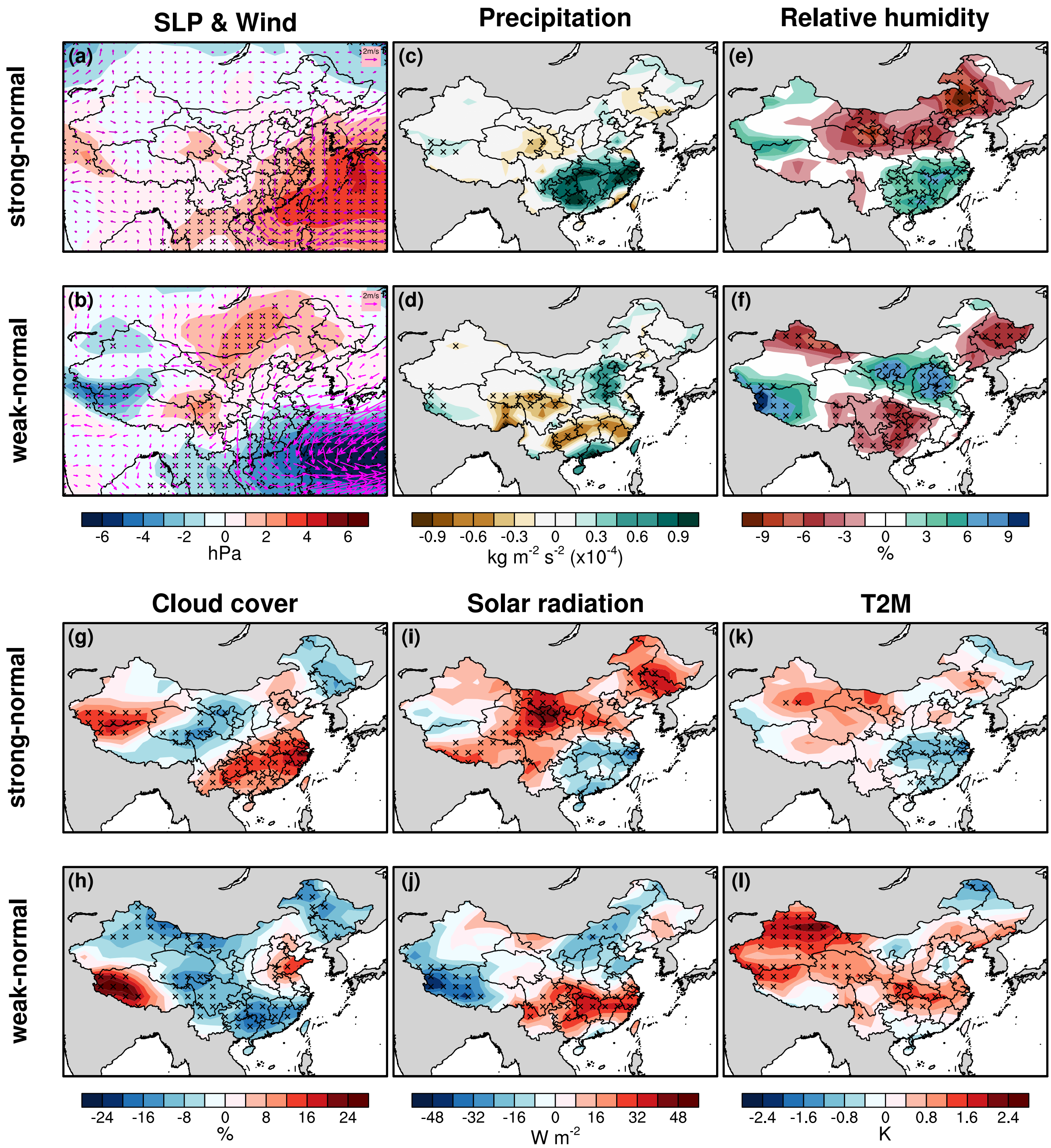

Figure 3. The difference of composite meteorological fields between different WPSH types. The first row corresponds to the difference between strong and normal WPSH days, and the second row correspond to the difference between weak and normal WPSH days. The meteorological variables including SLP, wind, precipitation, relative humidity, cloud cover, solar radiation, and 2 m temperature. The cross symbols indicate grids with significant levels less than 0.05 from Student's *t*-test.

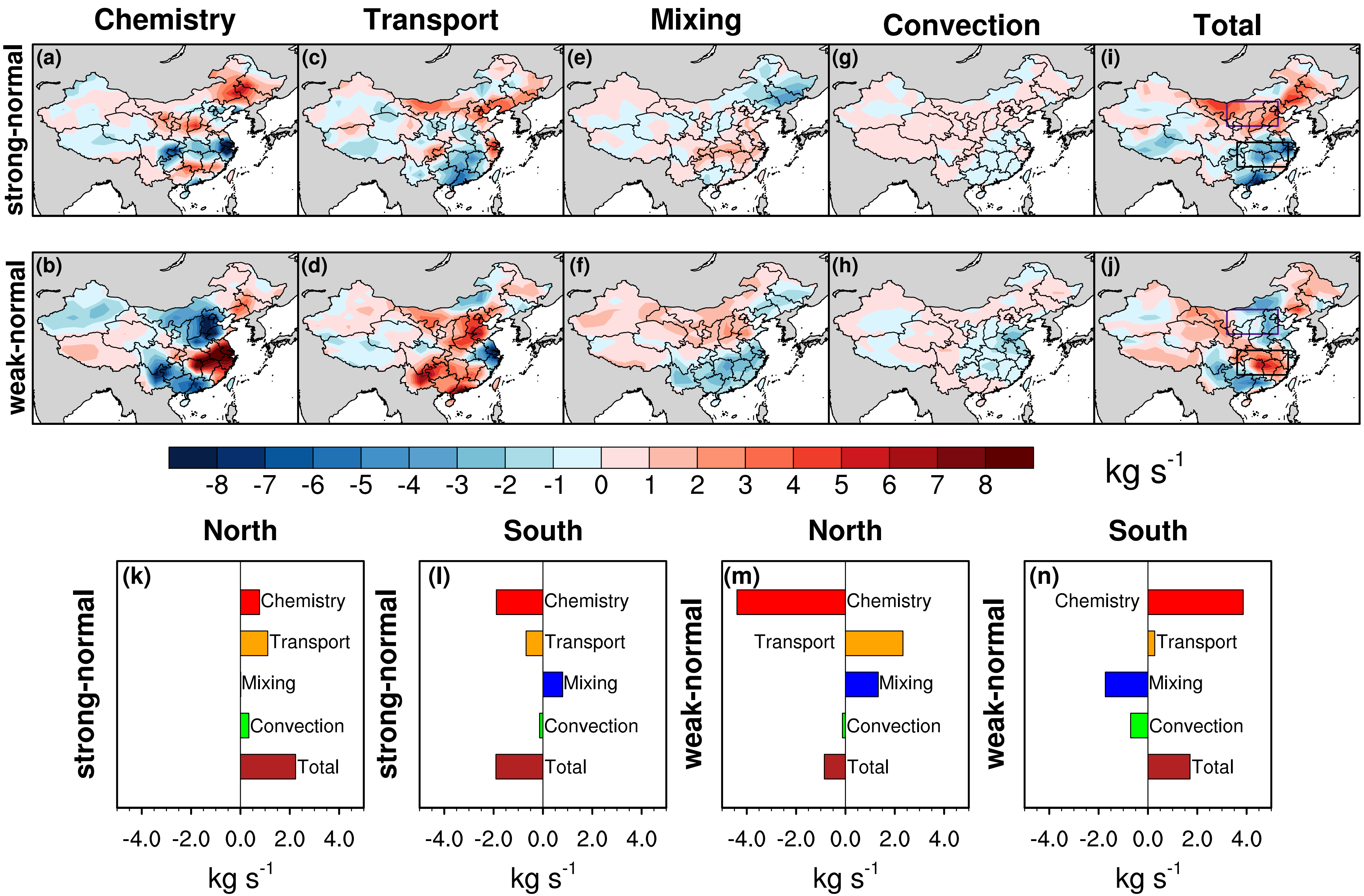

Figure 4. The budget diagnostics (kg s^{-1}) including chemistry, transport, mixing, and convection in the GEOS-Chem model. (a-j) The first row shows the differences between strong and normal WPSH days and the second row shows the differences between weak and normal WPSH days. (k-n) The area-averaged budget diagnostics (kg s^{-1}) for a north (36.0-42.0°N, 105.0-117.5°E) and south (26.0-32.0°N, 107.5-120.0°E) region (purple and black boxes in (i) and (j)).

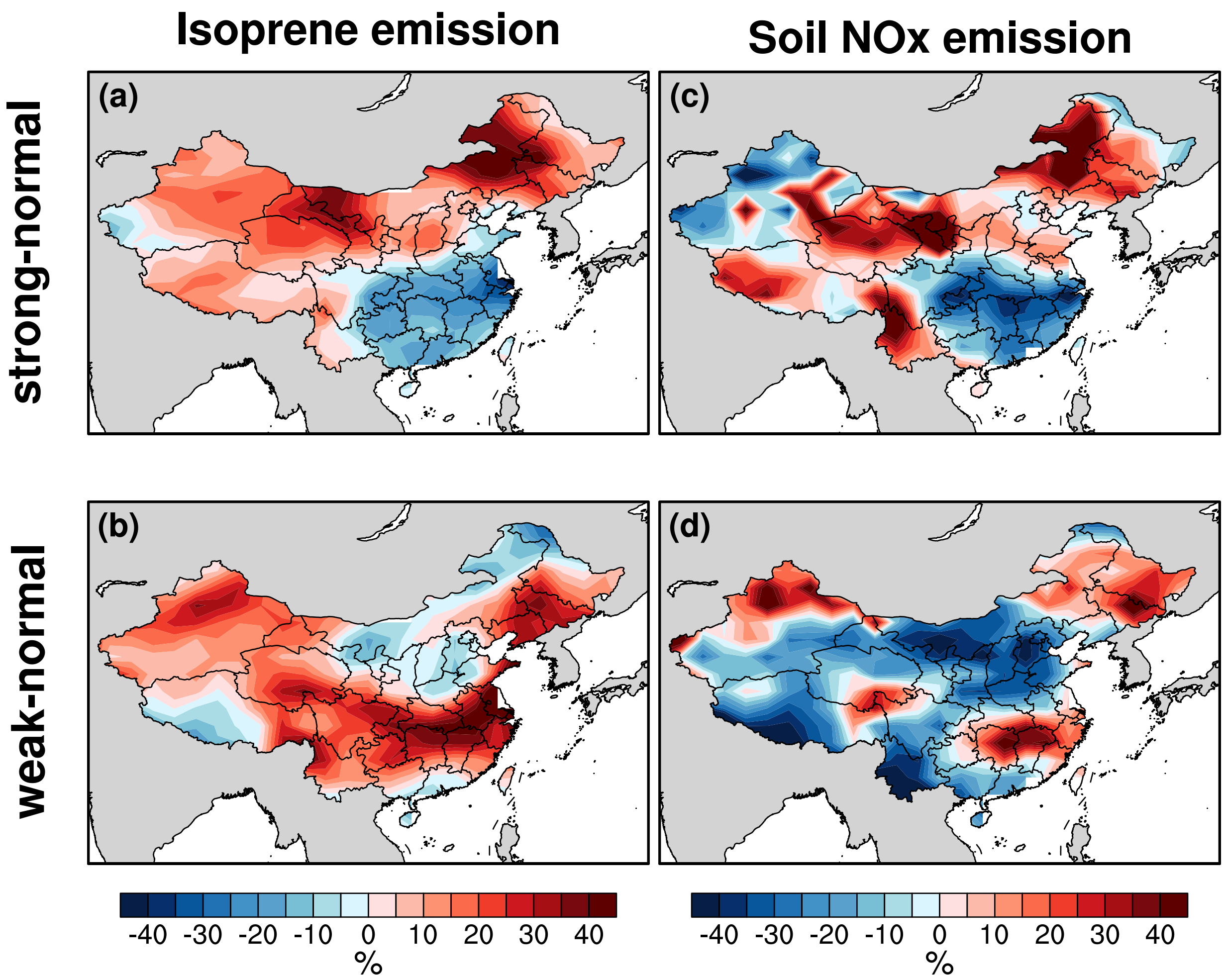

Figure 5. The changes of isoprene (a proxy of biogenic emission), soil NOx emission in GEOS-Chem model. The first row shows the relative differences (percentage) between strong and normal WPSH conditions and the second row shows those between weak and normal WPSH conditions.

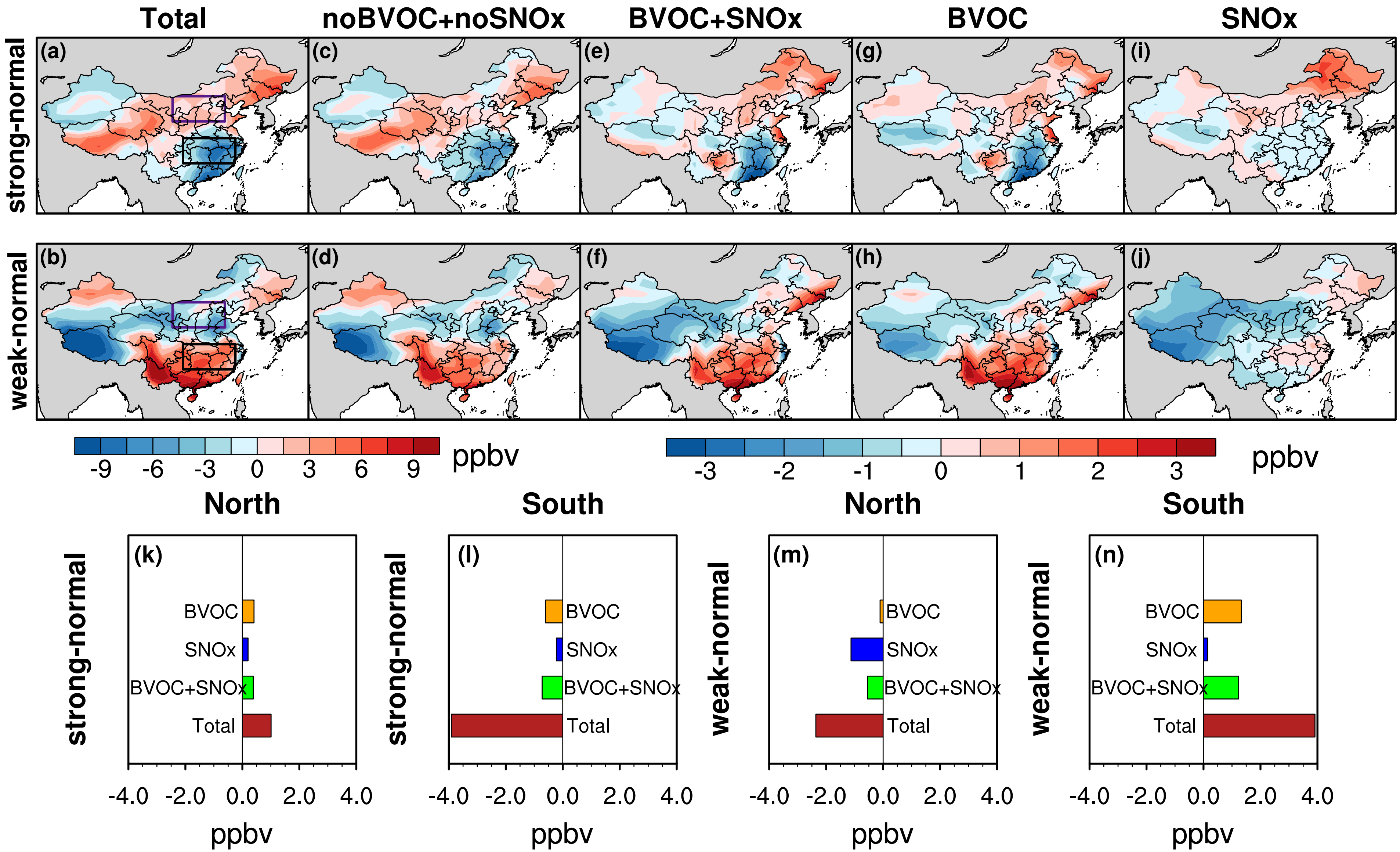

Figure 6. (a) and (b) show the simulated difference of MDA8 (ppbv) of strong and weak WPSH relative to normal WPSH, same as Figure 2a&b (filled contours). (c) and (d) are the same as (a) and (b) except turning off MEGAN and soil NOx emission. (e) and (f) show the difference between simulations with MEGAN and soil NOx emission on (Figure 6a&b) and off (Figure 6c&d), which represent the contribution of BVOC and soil NOx. (g) and (h) show the difference between simulations with MEGAN emission turned on and off, which represent the contribution of BVOC emission. (i) and (j) show the difference between simulations with soil NOx emission turned on and off, which represent the contribution of soil NOx emission. Note that (a-d) use the left colorbar and (e-j) use the right colorbar. (k-n) The contribution of BVOC, soil NOx (SNOx), BVOC together with soil NOx (BVOC+SNOx) for a north (36.0-42.0°N, 105.0-117.5°E) and south (26.0-32.0°N, 107.5-120.0°E) region (purple and black boxes in (a) and (b)).